NANO LETTERS

pubs.acs.org/NanoLett
Letter

Amphiphiles Formed from Synthetic DNA-Nanomotifs Mimic the Stepwise Dispersal of Transcriptional Clusters in the Cell Nucleus

Xenia Tschurikow,[#] Aaron Gadzekpo,[#] Mai P. Tran, Rakesh Chatterjee, Marcel Sobucki, Vasily Zaburdaev, Kerstin Göpfrich, and Lennart Hilbert*

Cite This: *Nano Lett.* 2023, 23, 7815–7824
Read Online

ACCESS | Metrics & More | Article Recommendations | Supporting Information

ABSTRACT: Stem cells exhibit prominent clusters controlling the transcription of genes into RNA. These clusters form by a phase-separation mechanism, and their size and shape are controlled via an amphiphilic effect of transcribed genes. Here, we construct amphiphile-nanomotifs purely from DNA, and we achieve similar size and shape control for phase-separated droplets formed from fully synthetic, self-interacting DNA-nanomotifs. Increasing amphiphile concentrations induce rounding of droplets, prevent droplet fusion, and, at high concentrations, cause full dispersal of droplets. Super-resolution microscopy data obtained from zebrafish embryo stem cells reveal a comparable transition for transcriptional clusters with increasing transcription levels. Brownian dynamics and lattice simulations further confirm that the addition of amphiphilic particles is sufficient to explain the observed changes in shape and size. Our work reproduces key aspects of transcriptional cluster formation in biological cells using relatively simple DNA sequence-programmable nanostructures, opening novel ways to control the mesoscopic organization of synthetic nanomaterials.

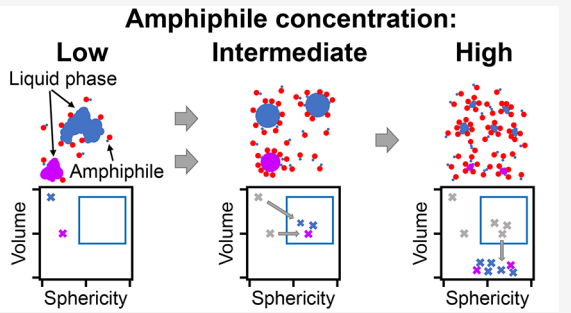

KEYWORDS: *DNA nanotechnology, Cell nucleus, Synthetic biology, Phase separation, Biomolecular condensates, Microemulsion*

Biological cells need to compartmentalize their molecular components to ensure their proper function. Conventionally, such compartmentalization is attributed to cellular organelles that are enclosed by membranes. More recently, processes based on liquid−liquid phase separation (LLPS) resulting from transient interactions were implicated in subcellular compartmentalization in biomolecular condensates.[1−3] The transfer of biologically inspired compartmentalization via LLPS into biomimetic and synthetic systems yields remarkable design possibilities and performance increase.[4] One example, a recently developed platform for fully programmable, multispecies phase separation is now available via DNA-nanomotifs, whose interactions are based on homology of "sticky ends" of exposed, self-complementary single-stranded DNA.[5,6] This platform has enabled the construction of a synthetic DNA segregation module that mimics chromosome separation during mitosis.[7] Embedding into DNA-nanomotif condensates has also allowed the combinatorial detection of tumor biomarkers and up to 20-fold acceleration of DNA-based logic gates.[8,9]

Condensates formed by canonical LLPS, commonly referred to as droplets, coarsen into increasingly larger droplets over time, whereas intracellular condensates are typically size-limited, or, in a state of microphase separation.[3,10,11] Size-limited condensates can be established and maintained by different physical mechanisms, including active reaction processes,[12,13] targeted removal of aged condensates,[14] or by provision of pinning centers at which condensates are localized.[15,16] Most commonly, however, microphase separation is attained by the addition of amphiphilic particles characterized by a dual affinity for two separating particle species.[17] Size-control by amphiphiles can be seen in several biological example cases.[18−20] A particularly well-studied case is the compartmentalization of transcription inside of the cell nucleus. One prominent example is RNA polymerase II (Pol II), the enzyme complex responsible for transcribing most eukaryotic genes, which acts as a bivalent connecting particle between microphase-separated domains enriched in either DNA or RNA.[21−26] An amphiphilic effect of ongoing transcription can also be seen by super-resolution microscopy of clusters of transcriptional machinery in stem cells.[27,28] These clusters form by a phase-separation mechanism[29−36] and unfold or even split into smaller clusters when they are engaged by genes that undergo transcriptional activation.[27,37] This effect can be reproduced in detail by a polymer model, in

Received: April 6, 2023
Revised: July 28, 2023
Published: August 16, 2023

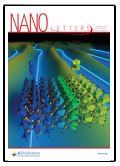

https://doi.org/10.1021/acs.nanolett.3c01301
Nano Lett. 2023, 23, 7815−7824

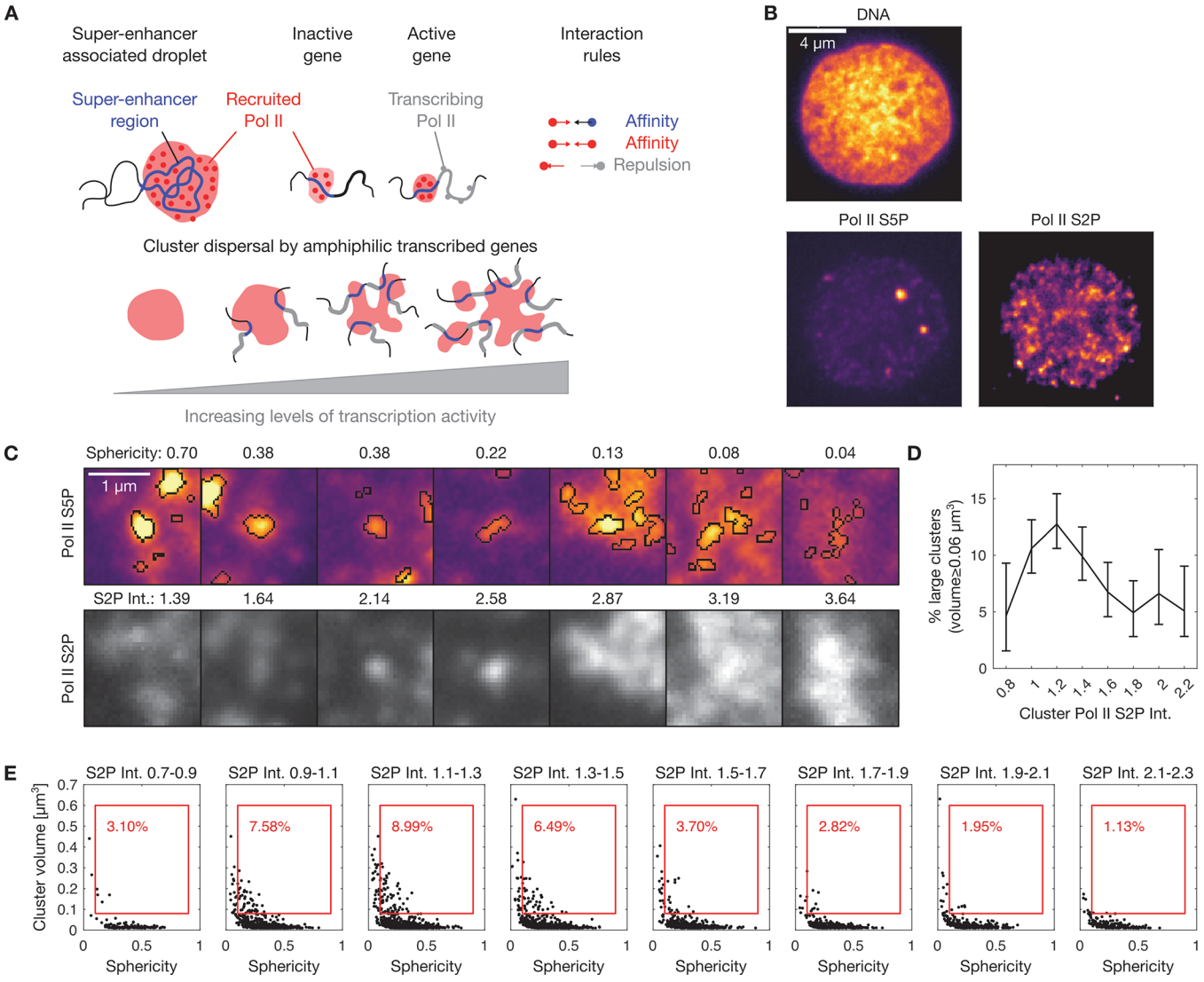

Figure 1. Transcribed genes act as amphiphile-like complexes that mediate the dispersal of RNA polymerase II clusters in nuclei of pluripotent zebrafish embryos. A) Illustration of the formation of clusters of recruited RNA polymerase II at super-enhancer regions of the genome and dispersal of clusters by an amphiphilic effect of transcribed genes. B) Representative three-color micrograph of an optical section through the middle of a cell nucleus in a pluripotent zebrafish embryo (sphere stage of development). Image data obtained by instant-SIM microscopy, color channels show DNA (Hoechst 33342), recruited RNA polymerase II (Pol II S5P, labeled by indirect immunofluorescence), and elongating RNA polymerase II (Pol II S2P, indirect immunofluorescence). C) Detail views of clusters of recruited RNA polymerase II, showing only the Pol II S5P and Pol II S2P channels. Segmentation was carried out in the Pol II S5P channel, as indicated in the top row. Sphericity was obtained from threshold-based segmentation of Pol II S5P clusters, S2P Int. refers to the mean intensity in the Pol II S2P channel, normalized by the median intensity of the nucleus that the cluster is contained in. D) Per-bin calculation of the percentage of large clusters in a given bin (volumes of 0.08 μm^3 or more, mean with 95% bootstrap confidence interval, data obtained from 99 nuclei pooled from 8 embryos). E) Segmented clusters were binned according to Pol II S2P intensity to generate sphericity-volume distributions. The percentage in red indicates binned clusters with volume $\geq$0.08 μm^3 and sphericity $\geq$0.1 (red box).

which transcribed genes are described as amphiphiles that associate with transcriptional clusters that, in turn, form by a liquid condensation mechanism.[27] Here, we extend the synthetic DNA-nanomotif droplet platform by amphiphile-motifs and show that the effect of these amphiphile-motifs closely resembles key features of the dispersal of embryonic transcriptional clusters.

Dispersal of RNA Polymerase II Clusters by an Amphiphilic Effect of Transcribed Genes. To allow for the comparison of the effect of DNA-based amphiphiles against a biological model system, we first characterize how transcriptional clusters are affected by the amphiphilic effects exerted by the transcribed genes. In the zebrafish embryo, for a number of genes, transient visits to especially long-lived and prominent transcriptional clusters occur, which are tightly coupled with the transcriptional control of these genes by so-called "super-enhancers".[27,28,37] As genes engage with transcriptional clusters and transcript elongation begins, transcriptional clusters unfold or even split into multiple parts (Figure 1A). This effect has been attributed to an amphiphilic property of genes that undergo activation in association with these prominent transcriptional clusters: while these genes exhibit an increased tendency to associate with transcriptional clusters, the beginning of transcript elongation additionally drives the exclusion of these genes from the transcriptional cluster.[37]

https://doi.org/10.1021/acs.nanolett.3c01301
Nano Lett. 2023, 23, 7815−7824

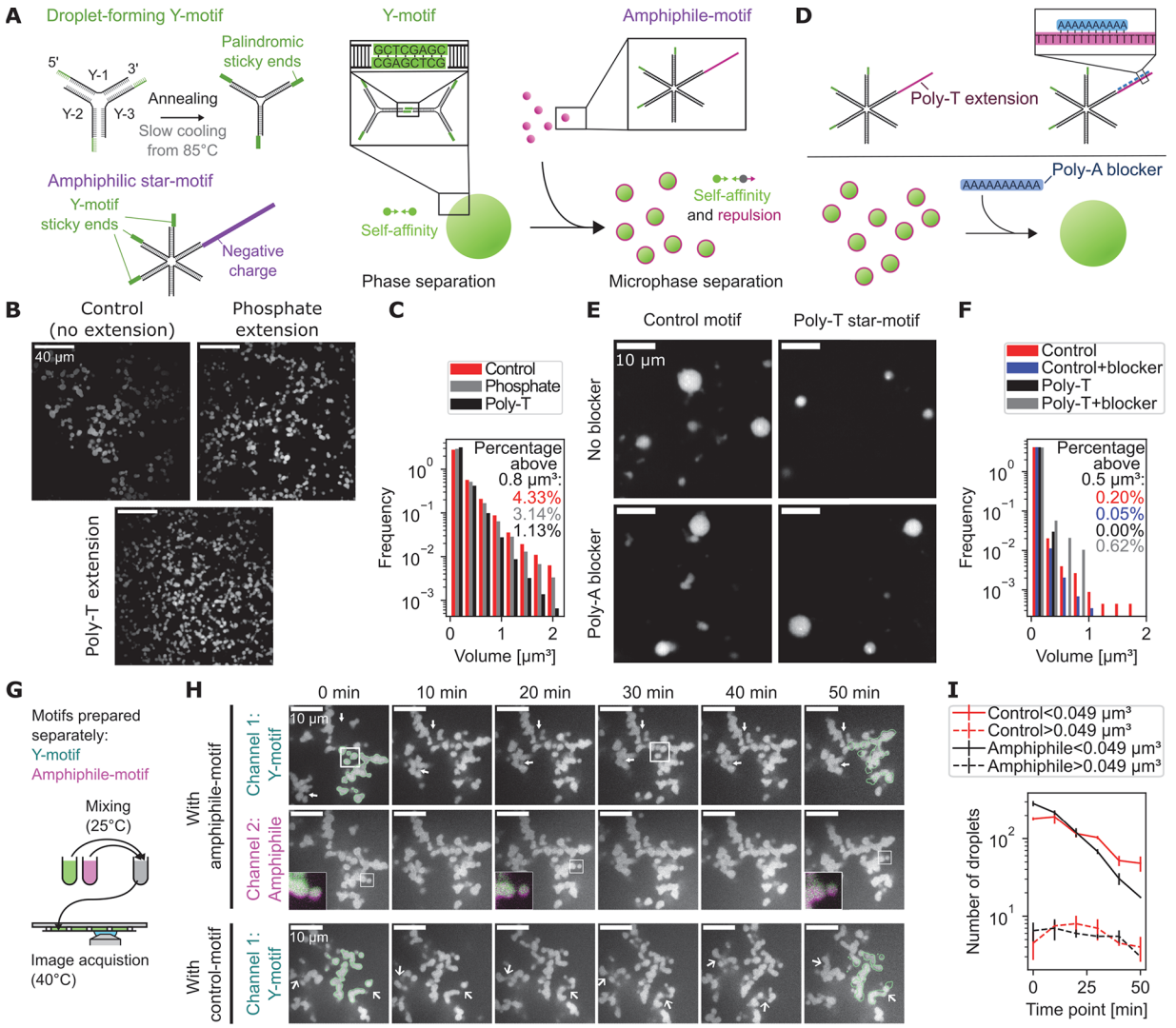

Figure 2. Amphiphiles for the dispersal of droplets formed from synthetic DNA-nanomotifs. A) Illustration of nanomotifs obtained by annealing of single DNA-oligomers, which consist of a 34 nt long core-structure, binding their neighboring strands, and an 8 nt long palindromic sticky end sequence. Amphiphile-motifs are generated by adding a repulsive extension to one vacant end of of a six-ended star motif. Y-motifs form phase-separated droplets due to the self-affinity established by sticky ends, which become dispersed upon the addition of amphiphile-motifs. B) Representative micrographs of Y-motif droplets in the presence of amphiphile-motifs. The negative charge is added via phosphate conjugation or the extension of one vacant end of the star-motif by 102 thymines (poly-T extension). Images are single confocal sections. C) Normalized histogram showing the size distribution of droplets with added control motifs, phosphate extension, or poly-T-extension. D) Illustration of the charge-canceling effect from adding 10 nt long poly-A blockers. E) Representative micrographs show single confocal sections of Y-motif droplets in the presence of star-motifs without (control-motif) or with poly-T extension (amphiphile-motif), without or with addition of poly-A blockers. F) Normalized histogram showing the effect of added poly-A blockers on the droplet volume distribution. G) Y-motif droplets and amphiphile-motif solution were prepared in separate reaction tubes and mixed together for time-lapse imaging of the subsequent reorganization processes. H) Representative two-color time-lapse showing single confocal sections obtained from volumetric image stacks originally acquired with a 1 min time interval. Images 3D-deconvolved (Lucy-Richardson), Y-motif channel corrected for photobleaching (exponential fit), insets were contrast-adjusted to emphasize local details. Results were comparable over two different frames per condition. I) Number of small (<0.049 μm^3) and large (>0.049 μm^3) droplets over time (n = 2, mean ± SEM).

To obtain a fine-grained assessment of how increasing transcription levels relate to the dispersal of transcriptional clusters in zebrafish embryos, we labeled different regulatory states of Pol II by immunofluorescence. Recruited RNA polymerase II, which serves as a label for transcriptional clusters, can be detected via a specific phosphorylation mark of the RNA polymerase II C-terminal domain (Pol II S5P, Figure 1B). A different phosphorylation mark (Pol II S2P) can be used to detect currently elongating Pol II, which serves as an indicator of ongoing transcript elongation (Figure 1B). Fluorescence images recorded by instant-SIM super-resolution confocal microscopy[38] revealed that the prominent Pol II S5P clusters were more unfolded and dispersed with higher levels of ongoing transcript elongation (Figure 1C). Assessing the fraction of large clusters at a given Pol II S2P level substantiates the impression that more large clusters occur at intermediate levels of transcript elongation (Pol II Ser2P intensity 1−1.4), and clusters disperse at high levels of transcript elongation (intensity >1.4) (Figure 1D). Quantifying the degree of unfolding via the sphericity of the Pol II S5P clusters also supports the impression that higher Pol II S2P levels correlate with a less spherical shape of the Pol II S5P

https://doi.org/10.1021/acs.nanolett.3c01301
Nano Lett. 2023, 23, 7815−7824

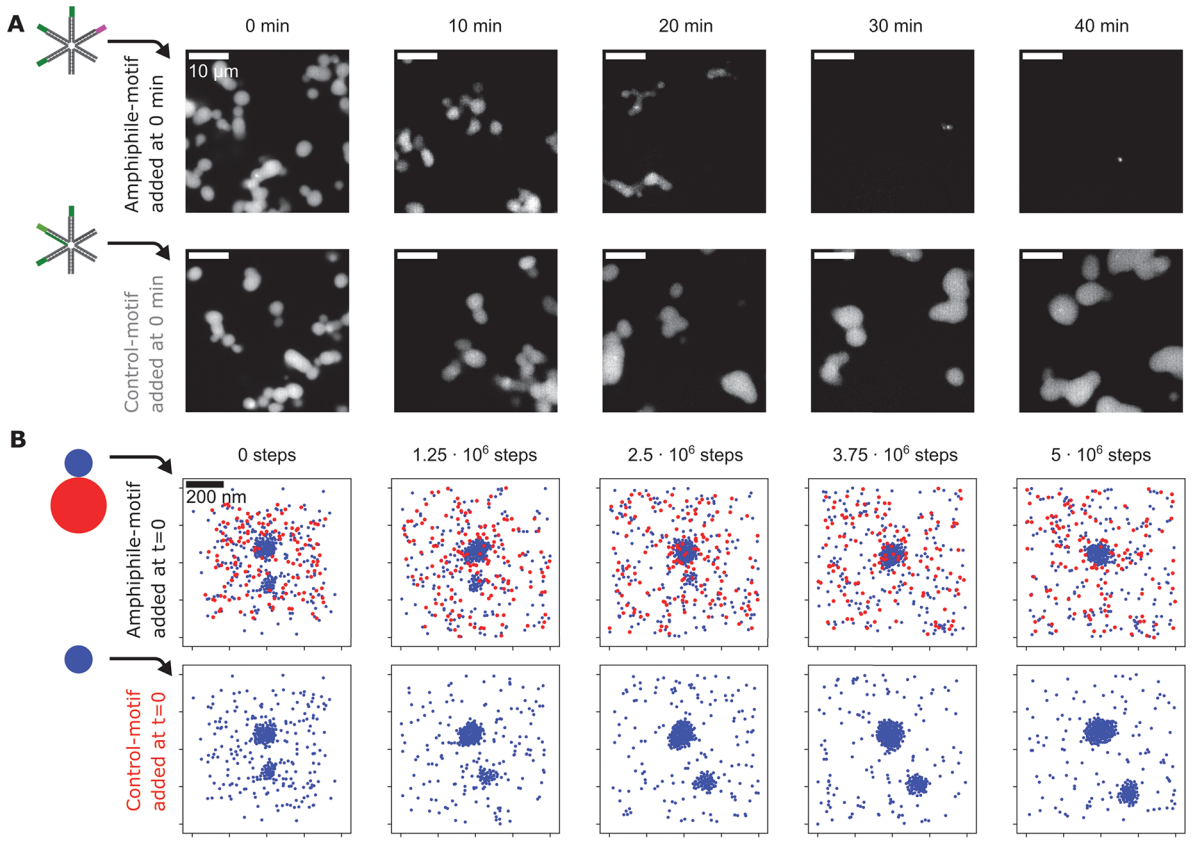

Figure 3. Time course of droplet dispersal upon addition of amphiphile-motifs. A) Representative confocal microscopy sections showing the distribution of Y-motifs in flow cells prepared at 10 min time intervals after amphiphile-motifs were added to preformed Y-motif droplets (0 min). Several tubes prepared in this manner were maintained at a stable temperature of 50 °C, control-motif samples were processed alongside amphiphile-motif experiments. B) To simulate the time-lapse experiment, either amphiphile-motifs or control-motifs were added to a simulation in a $1 \times 1 \times 1$ μm box containing preformed Y-motif droplets. Preformed droplets were generated by simulation with 450 Y-motifs for 10^6 steps at 60 °C. 450 amphiphile-motifs or control motifs (implemented as Y-motifs, displayed in blue) were then added, and 5×10^6 simulation steps at 40 °C were carried out. Images are 200 nm thick z-slices. Both simulations started from the same initial configuration.

clusters (Figure 1C). Indeed, a comprehensive overview of Pol II S5P cluster shape via sphericity-volume scatter plots revealed that a population of large (volume $\geq$ 0.08 μm^3) and round (sphericity $\geq$ 0.1) clusters is present specifically for intermediate levels of elongation activity (Figure 1E). At high levels of transcription, this population is reduced. Taken together, these analyses characterize how the amphiphilic effect of transcript elongation correlates with unfolding of transcriptional clusters and, at the highest levels of transcript elongation, loss of large clusters.

Amphiphile-Motifs Formed Purely from DNA can Disperse Droplets of Self-Interacting DNA-Nanomotifs. After characterization of the dispersal of transcriptional clusters as a biological reference for the desired amphiphilic effects, we proceeded to develop amphiphiles that disperse droplets formed from DNA-nanomotifs. The previously developed phase-separating DNA-nanomotifs, called Y-motifs due their three-ended shape, self-interact via sequence-programmed sticky ends.[5] Phase-separated Y-motif droplets can, in other words, also be correctly described as a conventional hydrogel formed on the basis of sequence-programmed bonds, for which bond length and experimental conditions were adjusted to obtain liquid droplet-like behavior. The viscosity and surface tension of Y-motif droplets was previously characterized by analysis of droplet fusion events,[5] which we supplemented with surface tension measurements by the sessile droplet method (5.2 $\pm$ 0.6 μN/m, mean $\pm$ SEM, see Materials and Methods).[39] Amphiphile-nanomotifs designed with the purpose of dispersing these droplets should also exhibit an affinity for the droplet-forming Y-motifs via sticky ends and, additionally, repulsion from the droplet phase (Figure 2A). Such a repulsion can be introduced, for example, by attaching negative charges via 5′-conjugation of a phosphate group, which resulted in a visually apparent reduction of droplet diameter, as is expected upon addition of an amphiphile (Figure 2B). An alternative approach to add negative charges for repulsion from the droplet phase, the extension by 102 thymines (poly-T extension), equally resulted in a visually apparent reduction of the droplet diameter (Figure 2B). Quantification by automated image analysis confirms that the fraction of droplets with large volumes (>0.27 μm^3) was lowered for star-motifs with phosphate extension, and even more so for star-motifs with poly-T extension (Figure 2C). As a result of the dispersive effect of the phosphate or poly-T extension, also the total number of droplets is increased compared to the control case (810 $\pm$ 40 and 1300 $\pm$ 100 versus 720 $\pm$ 30, respectively, mean $\pm$ SEM). We theorized that the poly-T-based dispersal was due to a generic charge-based exclusion of the added DNA from the phase-separated droplets, which can only be overcome when nanomotif-nanomotif interactions, i.e., complementary base pairing, facilitate the retention within droplets. In line with this

https://doi.org/10.1021/acs.nanolett.3c01301
Nano Lett. 2023, 23, 7815−7824

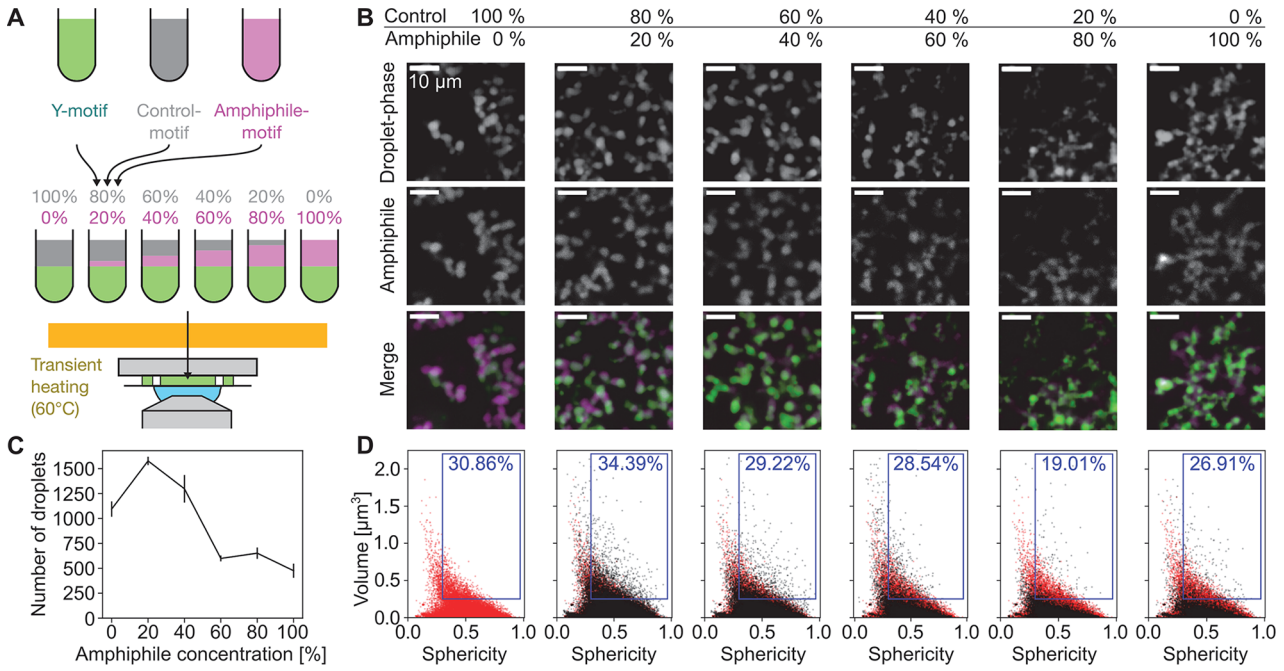

Figure 4. Increased amphiphile concentration leads to dispersal of phase-separated droplets. A) Y-motifs, control-motifs (no poly-T extension), and amphiphile-motifs were separately prepared, mixed at different percentages of amphiphile-motif, transiently heated (60 °C), and injected into flow cells for microscopy (ambient temperature 40 °C). B) Representative two-color micrographs of Y-motif and amphiphile-motif distributions at different amphiphile-motif concentrations. Micrographs are single confocal sections. C) Changes with amphiphile concentration of the number of droplets per field of view (mean ± SEM, n = 14, 14, 13, 13, 14, 14 fields of view). D) Sphericity-volume distributions obtained from the analysis of confocal image stacks (image stacks were acquired at up to five fields of view per sample, n = 15323, 22091, 18177, 7793, 8477, 6663 droplets, data pooled from N = 14, 14,13, 13,14, 14 total fields of view pooled from three independent experimental repeats). Small droplets (volume ≤ 0.125 μm^3) were excluded in calculation of percentages.

reasoning, the apparent dispersal of droplets by these amphiphile-motifs was abolished by the addition of 10 nt-long polyadenine (poly-A) blocker oligomers, which can facilitate transient poly-T-poly-T cross-linking by complementary base pairing, similar to the sticky ends (Figure 2D−F). We applied Dynamic Light Scattering (DLS) as an independent analytical method, thereby validating the dispersal of Y-motif droplets upon addition of poly-T-based amphiphile-motifs (droplet diameter 740 ± 50 nm vs 131 ± 3 nm, mean ± SEM, see Figure S1 and Materials and Methods). We used the poly-T-based amphiphile-motifs in the following steps of our study, as these amphiphile-motifs result in smaller droplets, and rely entirely on DNA-sequence effects, without chemical functionalization.

To better understand the dispersal of Y-motif droplets, we added amphiphile-motifs to a suspension containing preformed Y-motif droplets and visualized both species by time-lapse fluorescence microscopy (Figure 2G). At the beginning of the time-lapse, after an initial stablization for 45 min, Y-motifs as well as amphiphile-motifs are present in the droplets, with an amphiphile shell that extends slightly beyond the Y-motifs (Figure 2H, 0 min inset). Over the course of the time-lapse, fusion of individual droplets into larger droplets occurs, which is accompanied by an increase in the volume of the resulting droplets (Figure 2H, 20 min inset). Over time, several droplets fuse in this way, while separating gaps and holes between droplets also persist (Figure 2H, 50 min inset, arrows in row one). In comparison, droplets of Y-motifs to which control motifs were added also show droplet fusion, more frequently close gaps, and exhibit more rounded shapes compared to the droplets mixed with amphiphilic nanomotifs (Figure 2H, arrows in row three). These visual impressions suggest a difference in the maturation and dispersal of Y-motif droplets depending on the application of either the amphiphile-motif or the control-motif. Indeed, automated analysis of droplets revealed that small droplets are more rapidly lost in the presence of amphiphile-motifs, indicating dispersal of small droplets (Figure 2I). Further, the number of large droplets transiently increases in the presence of a control-motif, as is expected for canonical coarsening by fusion of, initially, small droplets into large droplets and then large droplets into a few even larger droplets (Figure 2I). In contrast, in the presence of amphiphile-motifs, the number of large droplets continuously decreases, as is expected when coarsening is prevented and droplets gradually become dispersed (Figure 2I).

Our initial results suggest that amphiphile-motifs are recruited to Y-motif droplets before they exert their dispersing effect. In a time-course experiment with more precise temperature control (50 °C), indeed, Y-motif droplets initially took on rounder shapes, became increasingly smaller only over time until, ultimately, most droplets vanished (Figure 3A). The addition of control-motifs that lack the poly-T extension also induced rounding of Y-motif droplets, while instead of becoming smaller, droplets continued to grow over time (Figure 3A).

We wanted to test whether attractive interactions between Y-motifs and amphiphile-motifs combined with a repulsive domain on the amphiphile-motifs are sufficient to explain these observations. We therefore implemented simulations based on Brownian dynamics, where Y-motifs were represented as spherical particles, which interact with other particles of the same kind via a harmonic well potential (Figure 3B, for an

https://doi.org/10.1021/acs.nanolett.3c01301
Nano Lett. 2023, 23, 7815−7824

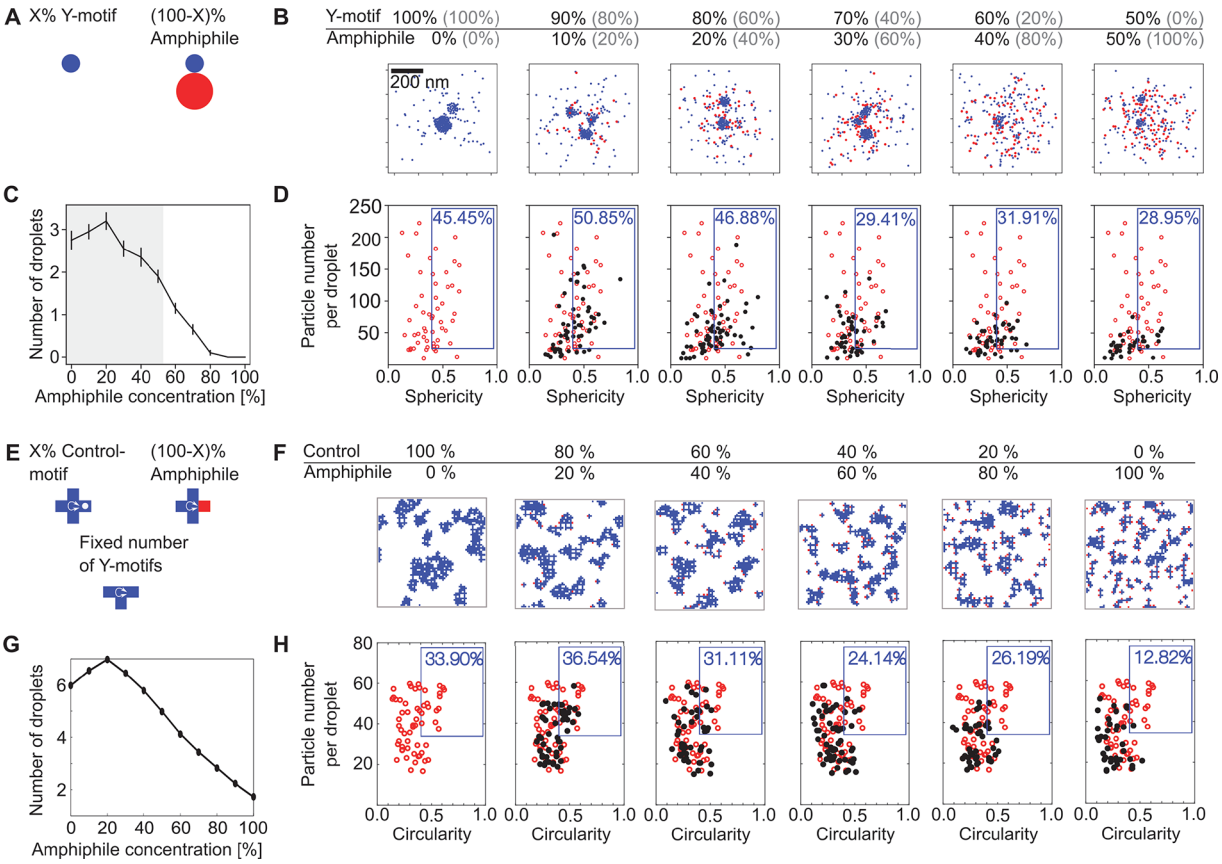

Figure 5. Amphiphile titration in interacting-particle and lattice simulations. A) To-scale drawing of Y-motifs and amphiphile-motifs used in the interacting-particle simulations. B) Particle-based simulations with 450 particles in total were used to represent the titration experiment. The fraction of amphiphile was increased from 0% to 100% in steps of 10%, the remaining fraction comprising of Y-motifs. Initially, all particles were distributed in a spherical volume (radius 200 nm) inside a simulation box of $1 \times 1 \times 1$ μm. 10^6 simulation steps were then carried out and the final configuration was evaluated. Due to the different methods of assigning percentages (number fractions in the simulation, volume fractions in the experiment), we provide corresponding percentages from the experiment in gray. One example of a z-slice (thickness 200 nm) of the final configuration is shown for each case. C) Number of droplets per simulation, gray regions correspond to the range investigated in the experiment, mean ± SEM (n = 20 simulations). D) Distributions of sphericity against particle number per droplet from 20 simulations. The blue box contains a percentage of droplets with sphericity higher than 0.4 and more than 25 particles per droplet. E) Lattice-based simulations with three different particle types were used to represent the titration experiment. T-shaped and cross-shaped DNA motifs perform diffusion and undergo stochastic rotation. Amphiphiles have one repulsive interacting arm (red), which is replaced by a neutral arm (white dot) for controls. F) Images show representative configurations of simulations carried out on 64 × 64 two-dimensional lattice. G) Number of droplets per simulation, mean ± SEM (n = 25 simulations). H) Distributions of circularity against particle number per droplet from 25 simulations. The percentage is for droplets with a circularity higher than 0.40 and more than 35 particles per droplet.

additional graphical summary, see Figure S2). Amphiphile-motifs are represented as composite particles comprising one "Y-motif particle" and one "tail particle", which experiences harmonic repulsion from all other particles. The interaction potentials were adjusted to recapitulate an experimentally observed transient increase in the number of droplets with increasing amphiphile-motif concentrations (Figure S3). We initialized a simulation with only Y-motifs, which we allowed to proceed until two differently sized droplets were formed, and subsequently added equal numbers of either amphiphile-motifs or control-motifs. The addition of amphiphile-motifs led to full dispersal of the smaller preformed droplet and prevented further growth of the larger droplet, whereas the addition of control-motifs resulted in continued growth for both droplets (Figure 3B). These observations already strongly indicated that indeed droplet dispersal can be attributed specifically to the repulsive poly-T tail. To consolidate these observations, we carried out a quantitative analysis of droplet number, volume, and sphericity for time-courses obtained experimentally and by simulation (Figure S4A–C and Figure S5A–C, respectively). In line with expectation, in both cases, the addition of amphiphile-motifs to preformed Y-motif droplets induces a transient increase in volume and sphericity, followed by full droplet dispersal. Adding control-motifs also leads to an increase in droplet volume and sphericity, and as expected, subsequent volume reduction and dispersal do not occur.

Addition of Increasing Amphiphile Concentrations Mimics the Dispersal of RNA Polymerase II Clusters. Having verified that amphiphile-motifs induce the expected droplet dispersal, we investigated whether they could be used to mimic the dispersal of transcriptional clusters with increasing levels of transcript elongation in zebrafish embryos. To imitate increasing levels of transcript elongation, we prepared mixtures of Y-motifs with increasing concentrations of amphiphile motifs (Figure 4A). In line with our previous observations, at all concentrations, amphiphile-motifs colocalized with Y-motif droplets, and higher amphiphile concentrations were associated with smaller droplets (Figure 4B). In

https://doi.org/10.1021/acs.nanolett.3c01301
Nano Lett. 2023, 23, 7815−7824

close agreement with observations made for Pol II clusters, also the droplet number transiently increases and then drops below the corresponding value without addition of amphiphile-motifs (Figure 4C). Also, the volume-sphericity distribution undergoes changes similar to those of Pol II clusters in zebrafish embryos for increasing levels of transcription (Figure 4D). In particular, the transient increase in the percentage of droplets with high volume and high sphericity mirrors the results for Pol II clusters. All observations were also visible in a second repeat of the titration experiment, indicating their reproducibility (Figure S6). Taken together, the changes in Y-motif droplets with increasing amphiphile-motif concentrations resemble the changes in Pol II clusters in zebrafish embryos for increasing levels of transcript elongation.

Finally, to assess whether our theoretical model can reproduce the dispersal of Y-motif droplets with increasing amphiphile-motif concentration, we simulated a titration experiment with increasing concentrations of amphiphile-motifs (Figure 5A). The volume fractions in the experiments with DNA-nanomotifs can be directly mapped to the particle number fractions in these simulations, and physical length scales are assigned to them, so that results from simulations can be thoroughly compared to the experiments (Figure 5B). Visually, an increase in the amphiphile-motif concentration leads to smaller Y-motif droplets and a more prominent accumulation of amphiphile-motifs on the surface of Y-motif droplets (Figure 5B). The number of detected droplets first rises and then drops, as seen in the experiments (Figure 5C). Sphericity-volume scatter plots show an increased fraction of large droplets with high sphericity, followed by a decrease in this fraction for even higher amphiphile-motif concentrations (Figure 5D). Taken together, our theoretical model largely captures the experimental observations for increasing concentrations of amphiphile-motifs, and, by extension, for transcriptional clusters with increasing levels of transcription.

To test the generality and robustness of our theoretical results, we implemented phenomenological lattice-based simulations including self-interacting particles and amphiphilic particles, thereby focusing on the essential interaction rules (Figure 5E). The simulation is accomplished on a 2-dimensional square lattice with different types of particles representing the different types of nanomotifs. Particles could not overlap and moved according to a dynamic Monte Carlo algorithm. Different affinities were assigned to the tips of the particles to represent the different nanomotifs. We consider three types of particles: three-armed particles with self-affinity analogous to the DNA Y-motifs; amphiphilic particles with an additional repulsive arm; and control particles similar to the amphiphiles, except that the additional arm is neutral (Figure 5E). Affinities and the particle density were adjusted so that self-interacting particles behave as a phase-separating liquid.[40−42] When we simulate the titration of amphiphile particles, large phase-separated domains are dispersed as the fraction of amphiphile particles increases, as seen in the interacting-particle simulations (Figure 5F). Further, a transient increase in droplet number and in the fraction of large round droplets is observed, in line with the interacting-particle simulations and experiments (Figure 5G,H). This agreement between lattice simulation and interacting-particle simulation results further supports that, indeed, the dispersal of phase-separated droplets by increasing amphiphile concentrations can be attributed to the same essential set of interaction rules. The robustness of our theoretical results is further supported by a quantitative analysis of the number of droplets, particle number per droplet, and circularity for time-lapse simulations, which matches experimental and interacting-particle simulation results (Figure S7).

Taken together, in all of the experimental and theoretical systems examined in this study, a stereotypical dispersal process was observed with increasing amphiphile concentrations. An increase in the fraction of large, round droplets and the total number of droplets can be observed at low amphiphile concentrations due to the prevention of droplet fusion and ripening. At sufficiently high amphiphile concentrations, droplets even become dispersed beyond the detection limit. In our understanding, this stereotypical behavior can be traced back to the similarity in the underlying amphiphile-mediated dispersal process. For low amphiphile levels, droplets grow as amphiphile particles are incorporated. Round, convex shapes become energetically favorable, as they maximize the distance between the repulsive, surface-attached parts of the amphiphile.[43] For increasing amphiphile concentrations, the requirement for increased droplet surface area to accommodate the additional amphiphile particles hinders droplet fusion and ripening and, ultimately, leads to dispersal of droplets.[17]

In summary, our results show how an amphiphilic DNA-nanomotif constructed solely on the basis of sequence interactions, without chemical functionalization, can be used to control the size of phase-separated droplet compartments or even induce complete dispersal of these compartments. While this controlled dispersal reproduces key aspects of the dispersal of transcriptional clusters in stem cells, several crucial features are not reflected in the synthetic DNA-motifs used in our study and could be considered in the future to achieve more realistic synthetic reimplementations of transcriptional clusters. Transcription in eukaryotes proceeds via several adjacent compartments at the scale of a few 100 nm, which harbor the consecutive steps of transcription control, transcript elongation, and splicing of the resulting transcripts.[44−48] The ability to implement several, orthogonally interacting DNA-motifs based on different sticky end sequences allows a similar formation of distinct droplet species, whose fusion and separation can be controlled by additional connector motifs.[5,7] The formation of transcriptional clusters in pluripotent cells involves super-enhancers as condensation surfaces,[27−32,45,49−53] whereas the Y-motif droplets in our study form without such condensation surfaces. Such surfaces could be provided by long DNA strands produced with the rolling circle amplification (RCA) method, which was previously used to generate DNA-only liquid droplets.[54] Lastly, the amphiphilic DNA-nanomotifs in our synthetic system are catalytically inactive, while the ongoing synthesis and transport of RNA can distinctly change the stability of transcriptional clusters[27,55] as well as the mesoscopic organization of different steps of the transcription process and chromatin.[21,56,57] In conclusion, our work illustrates how principles of intracellular compartmentalization can be translated into novel biomimetic concepts for the control of synthetic biological systems and materials.

■ ASSOCIATED CONTENT

Supporting Information

The Supporting Information is available free of charge at https://pubs.acs.org/doi/10.1021/acs.nanolett.3c01301

Materials and Methods; preparation, immunofluorescence staining, and imaging of zebrafish embryos;

https://doi.org/10.1021/acs.nanolett.3c01301
Nano Lett. 2023, 23, 7815−7824

design, preparation, and imaging of DNA-nanomotif suspensions; surface tension measurements; dynamic light scattering measurements; more details on interacting-particle simulations and lattice simulations; additional experimental repeats and quantification of cluster dispersal; supplementary references 5, 27, 38, 39, 58−68 (PDF)

AUTHOR INFORMATION

Corresponding Author

Lennart Hilbert − *Institute of Biological and Chemical Systems, Karlsruhe Institute of Technology, Eggenstein-Leopoldshafen 76344, Germany; Zoological Institute, Karlsruhe Institute of Technology, Karlsruhe 76131, Germany;* orcid.org/0000-0003-4478-5607; Email: lennart.hilbert@kit.edu

Authors

Xenia Tschurikow − *Institute of Biological and Chemical Systems, Karlsruhe Institute of Technology, Eggenstein-Leopoldshafen 76344, Germany; Zoological Institute, Karlsruhe Institute of Technology, Karlsruhe 76131, Germany*

Aaron Gadzekpo − *Institute of Biological and Chemical Systems, Karlsruhe Institute of Technology, Eggenstein-Leopoldshafen 76344, Germany; Zoological Institute, Karlsruhe Institute of Technology, Karlsruhe 76131, Germany*

Mai P. Tran − *Center for Molecular Biology of Heidelberg University (ZMBH), Heidelberg 69120, Germany; Max Planck Institute for Medical Research, Heidelberg 69120, Germany*

Rakesh Chatterjee − *Max Planck Zentrum für Physik und Medizin, Erlangen 91058, Germany; Chair of Mathematics in Life Sciences, Friedrich-Alexander Universität Erlangen-Nürnberg, Erlangen 91058, Germany*

Marcel Sobucki − *Institute of Biological and Chemical Systems, Karlsruhe Institute of Technology, Eggenstein-Leopoldshafen 76344, Germany*

Vasily Zaburdaev − *Max Planck Zentrum für Physik und Medizin, Erlangen 91058, Germany; Chair of Mathematics in Life Sciences, Friedrich-Alexander Universität Erlangen-Nürnberg, Erlangen 91058, Germany*

Kerstin Göpfrich − *Center for Molecular Biology of Heidelberg University (ZMBH), Heidelberg 69120, Germany; Max Planck Institute for Medical Research, Heidelberg 69120, Germany*

Complete contact information is available at: https://pubs.acs.org/10.1021/acs.nanolett.3c01301

Author Contributions

#X.T. and A.G. contributed equally

Notes

The authors declare no competing financial interest.

ACKNOWLEDGMENTS

We thank Juliana Pfeifer and the groups of Pavel Levkin and Ute Schepers for assistance and instrument access for Dynamic Light Scattering experiments. X.T., A.G., M.S., and L.H. are supported by the Helmholtz Program Natural, Artificial, and Cognitive Information Processing (NACIP). X.T. and L.H. received seed funding from the KIT Center Materials for Technical and Life Sciences (MaTeLiS). M.P.T and K.G. received funding by the Hector Fellow Academy, the Federal Ministry of Education and Research (BMBF), and the Ministry of Science Baden-Württemberg within the framework of the Excellence Strategy of the Federal, and State Governments of Germany and the Max Planck Society. R.C. and V.Z. were supported by the "Life?" initiative of the Volkswagen Stiftung.

REFERENCES

(1) Bergeron-Sandoval, L.-P.; Safaee, N.; Michnick, S. Mechanisms and Consequences of Macromolecular Phase Separation. *Cell* **2016**, *165*, 1067−1079.
(2) Shin, Y.; Brangwynne, C. P. Liquid phase condensation in cell physiology and disease. *Science* **2017**, *357*, eaaf4382.
(3) Lyon, A. S.; Peeples, W. B.; Rosen, M. K. A framework for understanding the functions of biomolecular condensates across scales. *Nat. Rev. Mol. Cell Biol.* **2021**, *22*, 215−235.
(4) Udono, H.; Gong, J.; Sato, Y.; Takinoue, M. DNA Droplets: Intelligent, Dynamic Fluid. *Advanced Biology* **2023**, *7*, 2200180.
(5) Sato, Y.; Sakamoto, T.; Takinoue, M. Sequence-based engineering of dynamic functions of micrometer-sized DNA droplets. *Science Advances* **2020**, *6*, eaba3471.
(6) Jeon, B. J.; Nguyen, D. T.; Saleh, O. A. Sequence-Controlled Adhesion and Microemulsification in a Two-Phase System of DNA Liquid Droplets. *J. Phys. Chem. B* **2020**, *124*, 8888−8895.
(7) Tran, M. P.; Chatterjee, R.; Dreher, Y.; Fichtler, J.; Jahnke, K.; Hilbert, L.; Zaburdaev, V.; Göpfrich, K. A DNA Segregation Module for Synthetic Cells. *Small* **2023**, *2202711*, 2202711.
(8) Gong, J.; Tsumura, N.; Sato, Y.; Takinoue, M. Computational DNA Droplets Recognizing miRNA Sequence Inputs Based on Liquid-Liquid Phase Separation. *Adv. Funct. Mater.* **2022**, *32*, 2202322.
(9) Do, S.; Lee, C.; Lee, T.; Kim, D. N.; Shin, Y. Engineering DNA-based synthetic condensates with programmable material properties, compositions, and functionalities. *Science Advances* **2022**, *8*, eabj1771.
(10) Klier, J.; Tucker, C. J.; Kalantar, T. H.; Green, D. P. Properties and Applications of Microemulsions. *Adv. Mater.* **2000**, *12*, 1751−1757.
(11) Hildebrand, E. M.; Dekker, J. Mechanisms and Functions of Chromosome Compartmentalization. *Trends Biochem. Sci.* **2020**, *45*, 385−396.
(12) Zwicker, D.; Hyman, A. A.; Jülicher, F. Suppression of Ostwald ripening in active emulsions. *Phys. Rev. E* **2015**, *92*, 012317.
(13) Michieletto, D.; Colì, D.; Marenduzzo, D.; Orlandini, E. Nonequilibrium theory of epigenomic microphase separation in the cell nucleus. *Phys. Rev. Lett.* **2019**, *123*, 228101.
(14) Narayanan, A.; Meriin, A.; Andrews, J O.; Spille, J.-H.; Sherman, M. Y; Cisse, I. I A first order phase transition mechanism underlies protein aggregation in mammalian cells. *eLife* **2019**, *8*, e39695.
(15) Berry, J.; Weber, S. C.; Vaidya, N.; Haataja, M.; Brangwynne, C. P. RNA transcription modulates phase transition-driven nuclear body assembly. *Proc. Natl. Acad. Sci. U.S.A.* **2015**, *112*, E5237−E5245.
(16) Zwicker, D.; Decker, M.; Jaensch, S.; Hyman, A. A.; Julicher, F. Centrosomes are autocatalytic droplets of pericentriolar material organized by centrioles. *Proc. Natl. Acad. Sci. U.S.A.* **2014**, *111*, E2636−E2645.
(17) Larson, R. G.; Scriven, L. E.; Davis, H. T. Monte Carlo simulation of model amphiphile-oil-water systems. *J. Chem. Phys.* **1985**, *83*, 2411−2420.
(18) Kelley, F. M.; Favetta, B.; Regy, R. M.; Mittal, J.; Schuster, B. S. Amphiphilic proteins coassemble into multiphasic condensates and act as biomolecular surfactants. *Proc. Natl. Acad. Sci. U.S.A.* **2021**, *118*, e2109967118.
(19) Samanta, N.; Ribeiro, S. S.; Becker, M.; Laborie, E.; Pollak, R.; Timr, S.; Sterpone, F.; Ebbinghaus, S. Sequestration of Proteins in Stress Granules Relies on the In-Cell but Not the In Vitro Folding Stability. *J. Am. Chem. Soc.* **2021**, *143*, 19909−19918.

(20) Cuylen, S.; Blaukopf, C.; Politi, A. Z.; Müller-Reichert, T.; Neumann, B.; Poser, I.; Ellenberg, J.; Hyman, A. A.; Gerlich, D. W. Ki-67 acts as a biological surfactant to disperse mitotic chromosomes. *Nature* **2016**, *535*, 308−312.
(21) Hilbert, L.; Sato, Y.; Kuznetsova, K.; Bianucci, T.; Kimura, H.; Jülicher, F.; Honigmann, A.; Zaburdaev, V.; Vastenhouw, N. L. Transcription organizes euchromatin via microphase separation. *Nat. Commun.* **2021**, *12*, 1360.
(22) Ricci, M.; Manzo, C.; García-Parajo, M. F.; Lakadamyali, M.; Cosma, M. Chromatin Fibers Are Formed by Heterogeneous Groups of Nucleosomes In Vivo. *Cell* **2015**, *160*, 1145−1158.
(23) Nozaki, T.; Imai, R.; Tanbo, M.; Nagashima, R.; Tamura, S.; Tani, T.; Joti, Y.; Tomita, M.; Hibino, K.; Kanemaki, M. T.; Wendt, K. S.; Okada, Y.; Nagai, T.; Maeshima, K. Dynamic Organization of Chromatin Domains Revealed by Super-Resolution Live-Cell Imaging. *Mol. Cell* **2017**, *67*, 282−293.e7.
(24) Ashwin, S. S.; Nozaki, T.; Maeshima, K.; Sasai, M. Organization of fast and slow chromatin revealed by single-nucleosome dynamics. *Proceedings of the National Academy of Sciences USA* **2019**, *116*, 19939−19944.
(25) Bintu, B.; Mateo, L. J.; Su, J. H.; Sinnott-Armstrong, N. A.; Parker, M.; Kinrot, S.; Yamaya, K.; Boettiger, A. N.; Zhuang, X. Super-resolution chromatin tracing reveals domains and cooperative interactions in single cells. *Science* **2018**, *362*, eaau1783.
(26) Szabo, Q.; Jost, D.; Chang, J. M.; Cattoni, D. I.; Papadopoulos, G. L.; Bonev, B.; Sexton, T.; Gurgo, J.; Jacquier, C.; Nollmann, M.; Bantignies, F.; Cavalli, G. TADs are 3D structural units of higher-order chromosome organization in Drosophila. *Sci. Adv.* **2018**, *4*, eaar8082.
(27) Pancholi, A.; Klingberg, T.; Zhang, W.; Prizak, R.; Mamontova, I.; Noa, A.; Sobucki, M.; Kobitski, A. Y.; Ulrich Nienhaus, G.; Zaburdaev, V.; Hilbert, L. RNA polymerase II clusters form in line with surface condensation on regulatory chromatin. *Mol. Syst. Biol.* **2021**, *17*, e10272.
(28) Klingberg, T.; Wachter, I.; Pancholi, A.; Gohar, Y.; Kumar, P.; Sobucki, M.; Kammer, E.; Eroğlu-Kayikçi, S.; Erhardt, S.; Ferrai, C.; et al. Transcriptional clusters follow a conserved condensation-dispersal sequence during stem cell differentiation. *bioRxiv* **2023**. DOI: 10.1101/2023.07.04.547621.
(29) Cho, W.-K.; Spille, J.-H.; Hecht, M.; Lee, C.; Li, C.; Grube, V.; Cisse, I. I. Mediator and RNA polymerase II clusters associate in transcription-dependent condensates. *Science* **2018**, *361*, 412−415.
(30) Guo, Y. E.; et al. Pol II phosphorylation regulates a switch between transcriptional and splicing condensates. *Nature* **2019**, *572*, 543−548.
(31) Sabari, B. R.; Dall'Agnese, A.; Boija, A.; Klein, I. A.; Coffey, E. L.; Shrinivas, K.; Abraham, B. J.; Hannett, N. M.; Zamudio, A. V.; Manteiga, J. C.; Li, C. H.; Guo, Y. E.; Day, D. S.; Schuijers, J.; Vasile, E.; Malik, S.; Hnisz, D.; Lee, T. I.; Cisse, I. I.; Roeder, R. G.; Sharp, P. A.; Chakraborty, A. K.; Young, R. A. Coactivator condensation at super-enhancers links phase separation and gene control. *Science* **2018**, *361*, eaar3958.
(32) Gibson, B. A.; Doolittle, L. K.; Schneider, M. W.; Jensen, L. E.; Gamarra, N.; Henry, L.; Gerlich, D. W.; Redding, S.; Rosen, M. K. Organization of Chromatin by Intrinsic and Regulated Phase Separation. *Cell* **2019**, *179*, 470−484.e21.
(33) Shrinivas, K.; Sabari, B. R.; Coffey, E. L.; Klein, I. A.; Boija, A.; Zamudio, A. V.; Schuijers, J.; Hannett, N. M.; Sharp, P. A.; Young, R. A.; Chakraborty, A. K. Enhancer Features that Drive Formation of Transcriptional Condensates. *Mol. Cell* **2019**, *75*, 549−561.
(34) Boehning, M.; Dugast-Darzacq, C.; Rankovic, M.; Hansen, A. S.; Yu, T.-K. T.; Marie-Nelly, H.; McSwiggen, D. T.; Kokic, G.; Dailey, G. M.; Cramer, P.; Darzacq, X.; Zweckstetter, M. RNA polymerase II clustering through carboxy-terminal domain phase separation. *Nature Structural and Molecular Biology* **2018**, *25*, 833−840.
(35) Shao, W.; et al. Phase separation of RNA-binding protein promotes polymerase binding and transcription. *Nat. Chem. Biol.* **2022**, *18*, 70−80.
(36) Lyons, H.; Veettil, R. T.; Pradhan, P.; Fornero, C.; De La Cruz, N.; Ito, K.; Eppert, M.; Roeder, R. G.; Sabari, B. R. Functional partitioning of transcriptional regulators by patterned charge blocks. *Cell* **2023**, *186*, 327−345.
(37) Hajiabadi, H.; Mamontova, I.; Prizak, R.; Pancholi, A.; Koziolek, A.; Hilbert, L. Deep-learning microscopy image reconstruction with quality control reveals second-scale rearrangements in RNA polymerase II clusters. *PNAS Nexus* **2022**, *1*, pgac065.
(38) York, A. G.; Chandris, P.; Nogare, D. D.; Head, J.; Wawrzusin, P.; Fischer, R. S.; Chitnis, A.; Shroff, H. Instant super-resolution imaging in live cells and embryos via analog image processing. *Nat. Methods* **2013**, *10*, 1122−1126.
(39) Ijavi, M.; Style, R. W.; Emmanouilidis, L.; Kumar, A.; Meier, S. M.; Torzynski, A. L.; Allain, F. H.; Barral, Y.; Steinmetz, M. O.; Dufresne, E. R. Surface tensiometry of phase separated protein and polymer droplets by the sessile drop method. *Soft Matter* **2021**, *17*, 1655−1662.
(40) Rotman, Z.; Eisenberg, E. Ideal glass transition in a simple two-dimensional lattice model. *Phys. Rev. E* **2009**, *80*, 060104.
(41) Chatterjee, R.; Segall, N.; Merrigan, C.; Ramola, K.; Chakraborty, B.; Shokef, Y. Motion of active tracer in a lattice gas with cross-shaped particles. *J. Chem. Phys.* **2019**, *150*, 144508.
(42) Merrigan, C.; Ramola, K.; Chatterjee, R.; Segall, N.; Shokef, Y.; Chakraborty, B. Arrested states in persistent active matter: Gelation without attraction. *Physical Review Research* **2020**, *2*, 013260.
(43) Klaiber, A.; Lanz, C.; Landsmann, S.; Gehring, J.; Drechsler, M.; Polarz, S. Maximizing Headgroup Repulsion: Hybrid Surfactants with Ultrahighly Charged Inorganic Heads and Their Unusual Self-Assembly. *Langmuir* **2016**, *32*, 10920−10927.
(44) Li, J.; Dong, A.; Saydaminova, K.; Chang, H.; Wang, G.; Ochiai, H.; Yamamoto, T.; Pertsinidis, A. Single-Molecule Nanoscopy Elucidates RNA Polymerase II Transcription at Single Genes in Live Cells. *Cell* **2019**, *178*, 491−506.e28.
(45) Li, J.; Hsu, A.; Hua, Y.; Wang, G.; Cheng, L.; Ochiai, H.; Yamamoto, T.; Pertsinidis, A. Single-gene imaging links genome topology, promoter−enhancer communication and transcription control. *Nature Structural and Molecular Biology* **2020**, *27*, 1032−1040.
(46) Forero-Quintero, L. S.; Raymond, W.; Handa, T.; Saxton, M. N.; Morisaki, T.; Kimura, H.; Bertrand, E.; Munsky, B.; Stasevich, T. J. Live-cell imaging reveals the spatiotemporal organization of endogenous RNA polymerase II phosphorylation at a single gene. *Nat. Commun.* **2021**, *12*, 3158.
(47) Ohishi, H.; Shimada, S.; Uchino, S.; Li, J.; Sato, Y.; Shintani, M.; Owada, H.; Ohkawa, Y.; Pertsinidis, A.; Yamamoto, T.; Kimura, H.; Ochiai, H. STREAMING-tag system reveals spatiotemporal relationships between transcriptional regulatory factors and transcriptional activity. *Nat. Commun.* **2022**, *13*, 7672.
(48) Cramer, P. Organization and regulation of gene transcription. *Nature* **2019**, *573*, 45−54.
(49) Morin, J. A.; Wittmann, S.; Choubey, S.; Klosin, A.; Golfier, S.; Hyman, A. A.; Jülicher, F.; Grill, S. W. Sequence-dependent surface condensation of a pioneer transcription factor on DNA. *Nat. Phys.* **2022**, *18*, 271−276.
(50) Quail, T.; Golfier, S.; Elsner, M.; Ishihara, K.; Murugesan, V.; Renger, R.; Jülicher, F.; Brugués, J. Force generation by protein−DNA co-condensation. *Nat. Phys.* **2021**, *17*, 1007−1012.
(51) Chong, S.; Dugast-Darzacq, C.; Liu, Z.; Dong, P.; Dailey, G. M.; Cattoglio, C.; Heckert, A.; Banala, S.; Lavis, L.; Darzacq, X.; Tjian, R. Imaging dynamic and selective low-complexity domain interactions that control gene transcription. *Science* **2018**, *361*, eaar2555.
(52) McSwiggen, D.; Hansen, A.; Teves, S.; Marie-Nelly, H.; Hao, Y.; Heckert, A.; Umemoto, K.; Dugast-Darzacq, C.; Tjian, R.; Darzacq, X. Evidence for DNA-mediated nuclear compartmentalization distinct from phase separation. *eLife* **2019**, *8*, e47098.
(53) Trojanowski, J.; Frank, L.; Rademacher, A.; Mücke, N.; Grigaitis, P.; Rippe, K. Transcription activation is enhanced by multivalent interactions independent of phase separation. *Mol. Cell* **2022**, *82*, 1878−1893.

https://doi.org/10.1021/acs.nanolett.3c01301
Nano Lett. 2023, 23, 7815−7824

(54) Liu, W.; Samanta, A.; Deng, J.; Akintayo, C. O.; Walther, A. Mechanistic Insights into the Phase Separation Behavior and Pathway-Directed Information Exchange in all-DNA Droplets. *Angew. Chem. Int. Ed.* **2022**, *61*, e202208951.
(55) Henninger, J. E.; Oksuz, O.; Shrinivas, K.; Sagi, I.; LeRoy, G.; Zheng, M. M.; Andrews, J. O.; Zamudio, A. V.; Lazaris, C.; Hannett, N. M.; et al. RNA-mediated feedback control of transcriptional condensates. *Cell* **2021**, *184*, 207−225.
(56) Nagashima, R.; Hibino, K.; Ashwin, S.; Babokhov, M.; Fujishiro, S.; Imai, R.; Nozaki, T.; Tamura, S.; Tani, T.; Kimura, H.; Shribak, M.; Kanemaki, M. T.; Sasai, M.; Maeshima, K. Single nucleosome imaging reveals loose genome chromatin networks via active RNA polymerase II. *J. Cell Biol.* **2019**, *218*, 1511.
(57) Feric, M.; Sarfallah, A.; Dar, F.; Temiakov, D.; Pappu, R. V.; Misteli, T. Mesoscale structure-function relationships in mitochondrial transcriptional condensates. *Proc. Natl. Acad. Sci. U.S.A.* **2022**, *119*, e2207303119.
(58) Chan, S. H.; Tang, Y.; Miao, L.; Darwich-Codore, H.; Vejnar, C. E.; Beaudoin, J. D.; Musaev, D.; Fernandez, J. P.; Benitez, M. D.; Bazzini, A. A.; Moreno-Mateos, M. A.; Giraldez, A. J. Brd4 and P300 Confer Transcriptional Competency during Zygotic Genome Activation. *Developmental Cell* **2019**, *49*, 867−881.e8.
(59) Hadzhiev, Y.; Qureshi, H. K.; Wheatley, L.; Cooper, L.; Jasiulewicz, A.; Van Nguyen, H.; Wragg, J. W.; Poovathumkadavil, D.; Conic, S.; Bajan, S.; Sik, A.; Hutvagner, G.; Tora, L.; Gambus, A.; Fossey, J. S.; Muller, F. A cell cycle-coordinated Polymerase II transcription compartment encompasses gene expression before global genome activation. *Nat. Commun.* **2019**, *10*, 691.
(60) Goldberg, I. G.; Allan, C.; Burel, J.-M.; Creager, D.; Falconi, A.; Hochheiser, H.; Johnston, J.; Mellen, J.; Sorger, P. K.; Swedlow, J. R. The Open Microscopy Environment (OME) Data Model and XML file: open tools for informatics and quantitative analysis in biological imaging. *Genome Biology* **2005**, *6*, R47.
(61) Schindelin, J.; et al. Fiji: an open-source platform for biological-image analysis. *Nat. Methods* **2012**, *9*, 676−682.
(62) Legland, D.; Arganda-Carreras, I.; Andrey, P. MorphoLibJ: integrated library and plugins for mathematical morphology with ImageJ. *Bioinformatics* **2016**, *32*, 3532−3534.
(63) Kestin, J.; Sokolov, M.; Wakeham, W. A. Viscosity of liquid water in the range- 8 to 150 C. *Journal of physical and chemical reference data* **1978**, *7*, 941−948.
(64) Yang, J.; Yu, K.; Zuo, Y. Y. Accuracy of axisymmetric drop shape analysis in determining surface and interfacial tensions. *Langmuir* **2017**, *33*, 8914−8923.
(65) Sato, Y.; Takinoue, M. Sequence-dependent fusion dynamics and physical properties of DNA droplets. *Nanoscale Advances* **2023**, *5*, 1919−1925.
(66) Jeon, B.-j.; Nguyen, D. T.; Abraham, G. R.; Conrad, N.; Fygenson, D. K.; Saleh, O. A. Salt-dependent properties of a coacervate-like, self-assembled DNA liquid. *Soft Matter* **2018**, *14*, 7009−7015.
(67) Hoffmann, M.; Fröhner, C.; Noé, F. ReaDDy 2: Fast and flexible software framework for interacting-particle reaction dynamics. *PLoS Computational Biology* **2019**, *15*, e1006830.
(68) Sato, Y.; Hilbert, L.; Oda, H.; Wan, Y.; Heddleston, J. M. J.; Chew, T.-L. T. L.; Zaburdaev, V.; Keller, P.; Lionnet, T.; Vastenhouw, N.; Kimura, H. Histone H3K27 acetylation precedes active transcription during zebrafish zygotic genome activation as revealed by live-cell analysis. *Development* **2019**, *146*, dev179127.

https://doi.org/10.1021/acs.nanolett.3c01301
Nano Lett. 2023, 23, 7815−7824